Check for updates

RESEARCH ARTICLE

NANO · MICRO small
www.small-journal.com

Size Dependent Phase Transformation of Liquid Gallium

Jinyun Liu, Lijian Song, Zidong He, Shengding Wang, Wuxu Zhang, Huali Yang, Fali Li, Shengbin Li, Jianing Wang, Huiyun Xiao, Dan Xu, Yiwei Liu, Yuanzhao Wu, Jun-Qiang Wang, Xiaoxue Shui, Yuan-Chao Hu, Jie Shang,* and Run-Wei Li**

As the most popular liquid metal (LM), gallium (Ga) and its alloys are emerging as functional materials due to their unique combination of fluidic and metallic properties near room temperature. As an important branch of utilizing LMs, micro- and submicron-particles of Ga-based LM are widely employed in wearable electronics, catalysis, energy, and biomedicine. Meanwhile, the phase transition is crucial not only for the applications based on this reversible transformation process, but also for the solidification temperature at which fluid properties are lost. While Ga has several solid phases and exhibits unusual size-dependent phase behavior. This complex process makes the phase transition and undercooling of Ga uncontrollable, which considerably affects the application performance. In this work, extensive (nano-)calorimetry experiments are performed to investigate the polymorph selection mechanism during liquid Ga crystallization. It is surprisingly found that the crystallization temperature and crystallization pathway to either α −Ga or β −Ga can be effectively engineered by thermal treatment and droplet size. The polymorph selection process is suggested to be highly relevant to the capability of forming covalent bonds in the equilibrium supercooled liquid. The observation of two different crystallization pathways depending on the annealing temperature may indicate that there exist two different liquid phases in Ga.

1. Introduction

Liquid metal is a special group of materials due to their unique combination of fluidic and metallic properties.[1] Gallium (Ga) and its alloys serve as promising liquid metals owing to their extremely wide liquid region, low toxicity, near-zero vapor pressure, and high thermal and electrical conductivity.[1–3] As an important branch of utilizing liquid metals, micro- and submicron-particles of Ga-based liquid metal have been fabricated by microfluidics, sonication and physical deposition, which are widely employed in wearable electronics, catalysis, energy, and biomedicine.[1,4–7] Meanwhile, the phase transition of Ga and its alloys is receiving increasing interest. A series of revolutionary technologies have been achieved by utilizing the reversible transformation of thermal, electrical, mechanical, and fluid characteristics during the liquid-solid phase transition process.[8–11] Besides, the phase transition determines the limiting temperature at which fluidic nature can be maintained.[12–14]

As the most important constituent, Ga has several solid phases under ambient pressure,[15,16] the stable phase is named α −Ga and the metastable phases have been reported as β −,[17] γ −,[18] δ −,[19] and ϵ −Ga.[20] The most obvious divergence between these phases is that α −Ga is partial covalent character,[15,16,21,22] while all the metastable phases are totally metallic.[16] The partial covalent character refers to the fact that there is only one of the seven bonds with the nearest neighbors is covalent in α −Ga (see **Figure 1**). This difference gives rise to a diversity of physical properties, such as metastable phases have lower melting points, melting enthalpies, and higher densities than stable phase. The generation of different phases is mainly related to their size of the particles.[23–26] Once the size decreases to micro-nano scale, higher undercooling could be provided. Actually, in such scenario, metastable phases β −, γ −, δ −Ga are preferred instead of stable α −Ga.[25–27] Therefore, the crystallization pathways and crystallization temperature of liquid Ga can differ remarkably at different length scales. However, this polymorph selection mechanism is still unclear, which considerably affects its application.[12–14]

Among all the metastable phases, β −Ga is the closest in energy to α −Ga[15,16] and most commonly obtained from the micro

J. Liu, L. Song, Z. He, S. Wang, W. Zhang, H. Yang, F. Li, S. Li, J. Wang, H. Xiao, D. Xu, Y. Liu, Y. Wu, J.-Q. Wang, X. Shui, J. Shang, R.-W. Li
CAS Key Laboratory of Magnetic Materials and Devices
Zhejiang Province Key Laboratory of Magnetic Materials and Application Technology
Ningbo Institute of Materials Technology and Engineering
Chinese Academy of Sciences
Ningbo 315201, P. R. China
E-mail: shangjie@nimte.ac.cn; runweili@nimte.ac.cn
J. Liu, R.-W. Li
School of Future Technology
University of Chinese Academy of Sciences
Beijing 100049, P. R. China
J. Liu, Z. He, W. Zhang, J. Wang, H. Xiao, D. Xu, R.-W. Li
Center of Materials Science and Optoelectronics Engineering
University of Chinese Academy of Sciences
Beijing 100049, P. R. China
Y.-C. Hu
Songshan Lake Materials Laboratory
Dongguan, Guangdong 523808, P. R. China
E-mail: yuanchao.hu@sslab.org.cn

The ORCID identification number(s) for the author(s) of this article can be found under https://doi.org/10.1002/smll.202305798

DOI: 10.1002/smll.202305798

 © 2023 Wiley-VCH GmbH

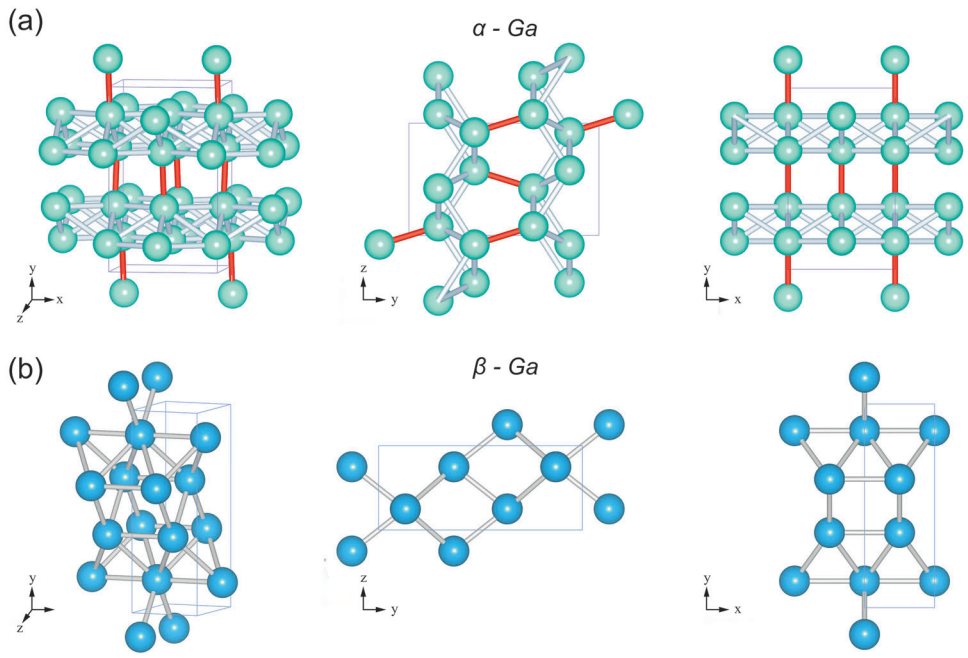

Figure 1. Characteristic crystal phases of Ga. a) The α −Ga in which metallic bonds (gray) and covalent bonds (red) co-exist. The crystal structure can be viewed as layers consisting of metallic bonds connected by covalent bonds. b) The β −Ga with only metallic bonds, which is a densely packed structure without any anisotropy. (see their physical properties difference in Table 1).

size liquid droplets.[17,27,28] Besides, the in situ transformation of α −Ga into β −Ga depending on the thermal history near the melting point of α −Ga is observed.[29,30] Thus it can be seen that size and thermal history may play a crucial role in the selection of crystallization pathways between stable and metastable phases. Additionally, knowledge about the liquid structure is necessary to understand the complex phase selection. Ga is a seemingly simple yet practically complex liquid with unusual behavior. Ga is an ice-type element when solidifies into α −Ga. The liquid state has attracted special interest for the anomalous configuration. This anomalous is related to the unusual covalency residue from α −Ga.[31,32] The temperature-dependent structure has been debated in experiments combining theoretical simulations.[33,34] Similar to the liquid–liquid phase transition (LLPT) hypothesis in the density anomalous system,[35–37] the LLPT has been proposed in high-pressure, undercooled liquid Ga confined in opal.[38–41] The evolution of liquid structure near the melting point and its impact on the selection of crystallization path requires more exploration.[42]

From the literature, the supercooling of Ga at small length scales has been attracting intensive research attentions in the past decades and there are a lot of interesting findings so far. For instance, the phase transformation and dynamics of Ga show significant size effect at the micron scale, including lower melting temperature and more pronounced supercooling effect of Ga particles at smaller sample size than the bulk samples.[43] It was also found by He et al.[23] that the formation of α −Ga and the metastable phases depends on the sample size. The authors studied small droplets and identified the size ranges for individual crystallization product. But how the supercooled liquid states affect such phase transformations coupled to the size effect is unexplored. Furthermore, an interesting phase separation phenomenon was observed at a much smaller length scale, that is in Ga-based alloy nanoparticles.[44] Thus a free-standing solid-core/liquid-shell structure could form. This hybrid structure will crystallize into different structures upon warming from low-temperature. This novel property may guide nano-engineering of liquid metals for diverse applications. In addition, because of its high thermal conductivity and large volume fusion enthalpy, Ga is considered as a promising phase change material. But its significant supercooling will increase the energy consumption, which requires suitable foreign nucleating agents to effectively reduce the supercooling.[45] Yunusa et al.[46] performed advanced experimental study on the structural ordering of supercooled liquid Ga. They revealed a possible liquid crystal mesophase by sandwiching Ga between polymer-coated glass substrates. Last but not the least, a recent study identifies that the passive oxide layer could protect the micron-size Ga from heterogeneous nucleation and greatly enhance the supercooling capability.[47] It provides important implications on the various applications of Ga, such as soft electronics and catalysis. These previous studies bring fascinating new knowledge on the properties of liquid Ga at different length scales. But the physical mechanism of the phase transformation of liquid Ga from various supercooled liquid states and sample sizes is still elusive.

In this work, we try to solve the above problems by carefully studying the phase transformation mechanism of Ga at different sample sizes using differential scanning calorimetry (DSC) and Flash DSC. We identified a universally existing critical annealing temperature that separates the polymorph selection mechanism. The liquid phase will crystallize into α −Ga below it otherwise into β −Ga. These results are explained from the perspective of the covalent bonds present in α −Ga while not in β −Ga. The significance of covalent bonds in the crystallization processes at

© 2023 Wiley-VCH GmbH

16136829, 0, Downloaded from https://onlinelibrary.wiley.com/doi/10.1002/smll.202305798 by Jie Shang - Ningbo Institute Of Materials , Wiley Online Library on [24/10/2023]. See the Terms and Conditions (https://onlinelibrary.wiley.com/terms-and-conditions) on Wiley Online Library for rules of use; OA articles are governed by the applicable Creative Commons License

16136829, 0, Downloaded from https://onlinelibrary.wiley.com/doi/10.1002/smll.202305798 by Jie Shang - Ningbo Institute Of Materials , Wiley Online Library on [24/10/2023]. See the Terms and Conditions (https://onlinelibrary.wiley.com/terms-and-conditions) on Wiley Online Library for rules of use; OA articles are governed by the applicable Creative Commons License

various sample sizes is discussed, as well as in the β −Ga to α −Ga solid–solid phase transformation. Our findings pave a new way to understand the unique physical properties of Ga and its phase transformation kinetics, offer new evidence for the transformation of liquid structure near melting point and provide further guidance on the design of new applications.

2. Results and Discussion

Figure 1 illustrates the crystal structures of α −Ga (a) and β −Ga (b).[17,48] For α −Ga, both non-directional metallic bonds and directional covalent bonds (highlighted with red color) exist. The crystal structure can be viewed as the layers of metallic bonds linked by the covalent bonds. For each Ga, it can have seven number of bonds, one of which is covalent. The appearance of this covalent bond grants fascinating properties for α −Ga and the liquid phase (see **Table 1** and below). On the contrary, the β −Ga only consists of metallic bonds, which gives rise to the isotropic densely-packed structure. As the physical properties are highly related to the material's structure, we list the typical physical properties of these two phases in Table 1.[16,17,30,48,49] Remarkably, α −Ga has a much higher melting temperature (T_m) demonstrating its better stability against thermal perturbation. It also has almost twice the enthalpy of fusion (ΔH_f) of metallic β −Ga, which indicates its larger driving force of crystallization. In fact, α −Ga is the equilibrium stable phase while β −Ga is the metastable one. Last but not least, α −Ga is less densely packed than β −Ga, which is evident from the lower mass density. These facts demonstrate the significance of introducing covalent bonds in Ga.

After noticing the importance of the covalent bonds in solid Ga, a question of how the liquid phase transforms into the different phases naturally arises. Even though the liquid phase is a single-component system, it may not be treated as a simple liquid.[50] To unravel the mystery of the crystallization pathway of liquid Ga, we designed a dedicated experimental strategy. In brief, as shown in **Figure 2**a, starting from a purified raw Ga droplet, we heat it to the liquid state at annealing temperatures T_{anneal} to relax for time t to reach the equilibrium state. The influence of holding time t on crystallization temperature T_{xtal} at different T_{anneal} is shown in Figure S1 (Supporting Information). We find that, the T_{xtal} shows almost no dependence on t ($t = 5$ min will be selected in all following tests). Then the liquid matter is quenched to the apparatus's low-temperature limit by using both conventional DSC and Flash DSC. Here, we want to introduce their main differences: the temperature window for Flash DSC is from 183 to 723 K. The chip-based Flash DSC is especially helpful for studying small size sample and can be operated in a substantially broadened scan range. The scan rates can reach 40 000 K s^{-1} in heating and 10 000 K s^{-1} in cooling. Conventional DSC is a powerful thermophysics investigations tool for bulk matter. Different sizes and types of crucibles can be selected according to experimental needs. The lower low-temperature window (123 K) makes conventional DSC more advantageous in ultra-low temperature thermal analysis. To study the sample size effect on the phase transformation, we combine these two experimental techniques. Finally, the formed solid phase is re-heated to a high-temperature to help measure the individual melting temperature of the solid phases and judge the final solid phase formed during cooling. We always keep the heating rate ϕ_h and cooling rate ϕ_c the same in an experimental cycle. With this optimized experimental protocol, we carried out extensive experiments on the Ga droplet of various sizes σ (μm).

Table 1. Characteristic physical properties of α −Ga and β −Ga, including melting temperature T_m, enthalpy of fusion ΔH_f, and density ρ.

Phase	T_m (K)	ΔH_f (kJ mol^{-1})	ρ (g cm^{-3})	Covalent bonding
α −Ga	302.9	5.58	5.92	Yes
β −Ga	256.8	2.65	6.22	No

We first show two exemplified results. First, Figure 2b demonstrates the heat flow curves from conventional DSC for droplet size ≈1014 μm. The results are differentiated from each other by the different T_{anneal}, ranging from 313 to 358 K, at the rate of $\phi_h = \phi_c = 0.083$ K s^{-1}. Note that conventional DSC has a much lower temperature limit than that of the Flash DSC (123 vs 183 K). In DSC scans, based on the melting temperature T_m and the enthalpy of fusion ΔH_f (see Table 1), we are able to judge the crystallization phases generated in the cooling process. However, defining the freezing point of Ga is by no means easy in our experiments because of many effects such as sample size or annealing temperature studied here. Interestingly, when T_{anneal} is low, the liquid phase shows only one exothermic peak during cooling and one endothermic peak corresponding to α −Ga melting during reheating. The crystallization process is simple as liquid → α. This crystallization temperature T_{xtal}(liquid → α) will decrease with the increasing T_{anneal} until a certain critical point we call T^*_{anneal}. Above T^*_{anneal}, the crystallization pathway is different. As we can see from Figure 2b, the liquid phase will instead crystallize into the metastable β −Ga and then the latter will transform to the stable α −Ga. These two steps are manifested by the double exothermic peaks during cooling. Nevertheless, the endothermic signal during reheating keeps unchanged. Furthermore, we find that the phase transformation temperature T_{xtal}(liquid → β) does not change with altering T_{anneal}. While T_{xtal}(β → α) do decrease with T_{anneal} in the current detection window. We note that T_{xtal}(β → α) will saturate at a higher T_{anneal} (see below).

Second, we show the results from Flash DSC of a smaller droplet ($\sigma \approx 128$ μm) in Figure 2c. Similar trends are observed as those from DSC curves in Figure 2b. However, when T_{anneal} is high enough, T_{xtal}(β → α) is hard to detect which may result from the limited low-temperature limit of Flash DSC (183 K). As a result, the reheating curve shows the melting behavior of β −Ga. Furthermore, we performed thorough experimental investigations at various heating and cooling rates. The results are depicted in Figure 2d. The collapse of the data from the rates over two orders of magnitude demonstrates the robustness of our findings. It becomes evident that the effect of the rate diminishes notably above T^*_{anneal}. In Figure 2d, the occasional observation of a solid–solid transition of β −Ga to α −Ga at a small sample size brings additional interest on the phase transformation behavior. There are two possible reasons for this occasional observation. On the one hand, as we can see from **Figure 3**, the crystallization temperature T_{xtal}(β → α) of β −Ga to α −Ga will decrease with decreasing sample size. It is experimentally very hard to detect when the sample size falls under 200 μm. Under this condition,

 © 2023 Wiley-VCH GmbH

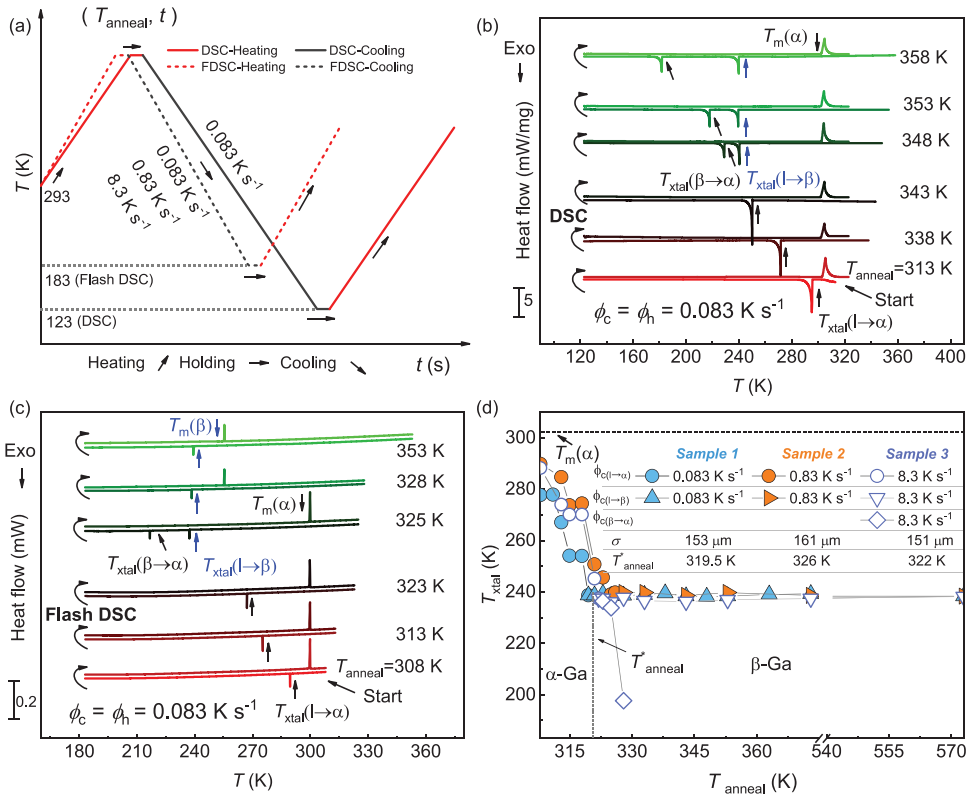

Figure 2. Calorimetry experimental protocols. a) Schematic plot of experimental design. Both Flash DSC and DSC are used based on the sample size. The low-temperature limits of Flash DSC and DSC are 183 and 123 K, respectively. The pre-processed sample will first be heated to T_{anneal} and relax for time t before being cooled back to the low-temperature. Finally, the solidified crystal will be heated back to the liquid state. We keep the cooling rate ϕ_c and heating rate ϕ_h the same. b) Experimental results from DSC for sample size ≈1014 μm. From the bottom to the top, the annealing temperature is 313, 338, 343, 348, 353, and 358 K, respectively. At low T_{anneal}, the liquid will transform to α −Ga directly, while β −Ga will form before α −Ga emerge at higher T_{anneal}. c) Similar experimental observations with (b) for $\sigma \approx$ 127 μm from Flash DSC experiments. The tested temperatures are 308, 313, 323, 325, 328, and 353 K from the bottom to the top. But the $\beta \rightarrow \alpha$ phase transformation is hard to detect at high T_{anneal}. d) The rate invariance of our experimental results. Both the observed liquid→ α and liquid→ β phase transformations do not depend on ϕ_h and ϕ_c.

$T_{xtal}(\beta \rightarrow \alpha)$ can approach 180 K or even lower with an uncertainty of 10 − 20 K, which is close to the lower temperature apparatus limit of Flash DSC (183 K). This can be further corroborated from Figure 3d in which $T_{xtal}(\beta \rightarrow \alpha)$ is close to 180 K at a sample size of 308 μm by conventional DSC. Meanwhile, the Flash DSC (Figure 3b) cannot detect such a phase transition because of its larger experimental difficulty and uncertainty. On the other hand, at small sample sizes, see Figure 3, the boundary of the solid-solid transition of β −Ga to α −Ga close to T^*_{anneal} (see definition below) is very sharp, which could increase the experimental uncertainty. In our experiments, we find that we usually need to use Flash DSC to make the measurements when sample size is <200 μm. This is why generally we cannot observe the solid–solid transition of β −Ga to α −Ga at small sample sizes, but only occasionally. In Figure 2d, our main purpose is to eliminate the cooling rate effect on our findings. That is, the influence of the cooling rate, at least in two orders of magnitude, is negligible on the polymorph selection behavior in the crystallization of liquid Ga. Therefore, we mainly performed experiments by focusing on changing cooling rates. Since, such an occasional observation does not affect any of our main findings, it is an interesting topic to investigate in the future to maximize the capability of Flash DSC in studying the crystallization kinetics of liquid Ga and that of the other materials. The results for another additional size ($\sigma \approx 130\,\mu m$) is shown in Figure S2 (Supporting Information).

Next, we investigate how this polymorph selection process depends on the droplet sizes σ. We show detailed outcomes in Figure 3 for various σ (128 − 1014 μm). Note that Figure 3a,b is from Flash DSC and the rest from conventional DSC. By careful inspection, several key features can be unearthed. As discussed above, T^*_{anneal} exists for each sample size and shows a non-trivial size dependence. When $T_{anneal} < T^*_{anneal}$, only liquid→ α happens and the transformation temperature T_{xtal}(liquid → α) decreases abruptly with increasing T_{anneal}. With T_{anneal} passing T^*_{anneal}, the β −Ga crystallization intervenes. The primary crystallization path is liquid→ β instead of liquid→ α. Because of the metastable nature of β −Ga, it will inevitably transform to α −Ga at a lower temperature. We also observed similar results by maintaining this high-temperature liquid ($T_{anneal} > T^*_{anneal}$) at room temperature for a period of time (see Figure S3, Supporting Information). This indicates that the liquid properties at room temperature are inherited from the equilibrium high temperature mother liquid. Interestingly, in the full annealing temperature range, the crystallization temperature T_{xtal}(liquid → β) does not change. Meanwhile, the solid–solid transformation temperature $T_{xtal}(\beta \rightarrow \alpha)$ also does not rely on T_{anneal} after the narrow transition stage close to T^*_{anneal}.

© 2023 Wiley-VCH GmbH

16136829, 0, Downloaded from https://onlinelibrary.wiley.com/doi/10.1002/smll.202305798 by Jie Shang - Ningbo Institute Of Materials , Wiley Online Library on [24/10/2023]. See the Terms and Conditions (https://onlinelibrary.wiley.com/terms-and-conditions) on Wiley Online Library for rules of use; OA articles are governed by the applicable Creative Commons License

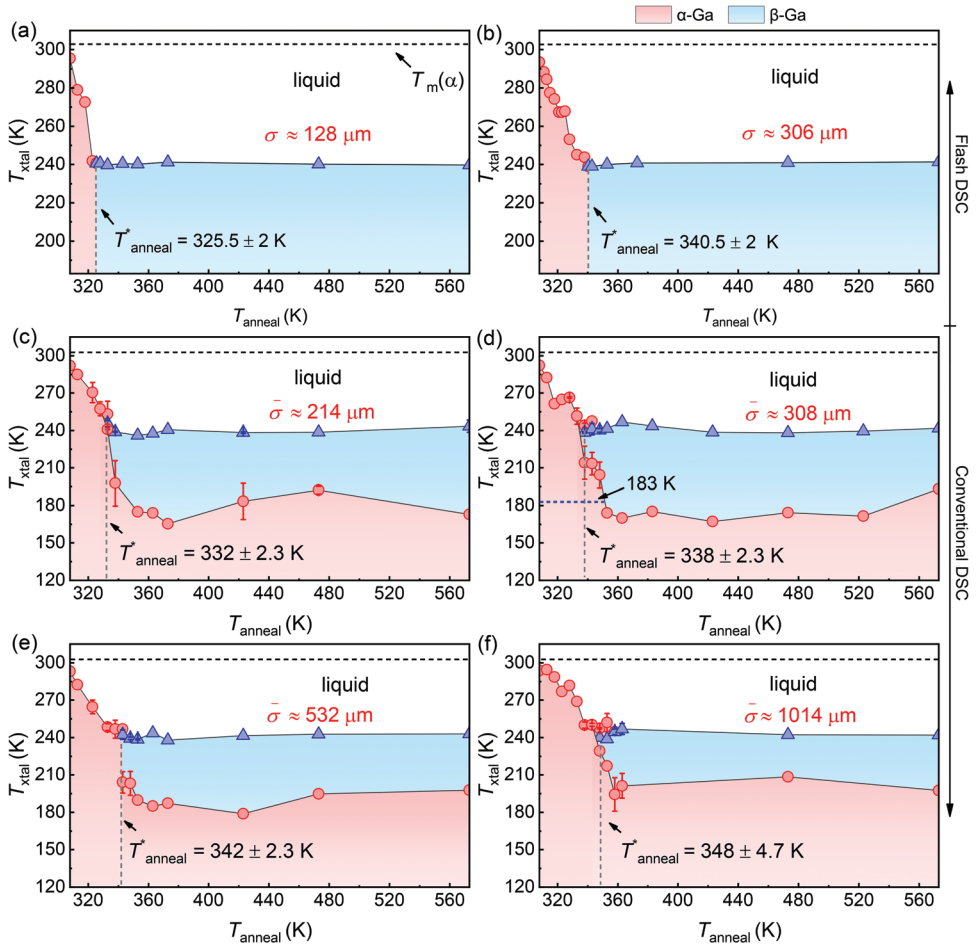

Figure 3. Size-dependent phase transformations. a,b) Flash DSC experimental results for $\sigma \approx 128$ μm and $\sigma \approx 306$ μm at $\phi_h = \phi_c = 0.083$ K s^{-1}. c–f) DSC results for average σ as 214, 308, 532, and 1014 μm, respectively, here the $\phi_h = \phi_c = 0.083$ K s^{-1}. In panel (d), the lower temperature limit of Flash DSC (183 K) is also included for better comparison. For all the studied sample sizes, there is a size-dependent critical annealing temperature T^*_{anneal}. When $T > T^*_{anneal}$, liquid → β happens otherwise liquid → α. The survival temperature window of the α −Ga from liquid → α transformation shrinks dramatically with reducing sample size. We notice that the transformation temperatures of liquid → β and β → α barely depend on T_{anneal}. Nevertheless, the latter shows non-negligible dependence on the sample size. The size σ in the Flash DSC measurement is the approximate size of one test sample, and in DSC results, σ represents the weighted average of the sample size corresponding to each annealing temperature.

In our experiments, we find that the fluctuations of T_{xtal}(liquid → α) and T_{xtal}(liquid → β) are small. These demonstrate the excellent repeatability of our experiments at different annealing temperatures for different sample sizes. While the solid–solid transition from β −Ga to α −Ga shows comparatively larger fluctuations, but generally good repeatability. Another important feature is the survival region of α −Ga defined by the temperature range up to T^*_{anneal} (the pink shade before the dashed line). Such a survival region shrinks dramatically with reducing sample size, which indicates the favor of α −Ga formation at larger sample sizes. We further emphasize the effective collaboration of Flash DSC and conventional DSC tests by the consistent results in Figure 3b,d. As aforementioned, $T_{xtal}(\beta \rightarrow \alpha)$ can be <183 K resulting in the absence of the corresponding exothermic peak in the Flash DSC curves (for example, see Figure 2c). The others extended sizes with similar results are shown in Figure S4 (Supporting Information). We also extend our experiments to the sample size up to about 3000 μm and found similar behaviors to Figure 3f (see Figure S5, Supporting Information). However, further extension to larger sample sizes suffer from some experimental difficulty from apparatus limits. In a recent work by Zhang et al.,[45] a similar trend of how the maximum temperature (similar to T_{anneal} here) affects the phase transformation behavior of Ga was observed. But lacking of the details of the sample size, sample shape, and sample type (powder or bulk etc.) makes it hard to for us to estimate their critical maximum temperature to identify the direct connection to our work. Additional experiments may be required to build such an intriguing connection.

To better illustrate these experimental measurements, we summarize our dataset in **Figure 4** by building up a 2D plot based on the droplet size σ and the annealing temperature T_{anneal}. The boundary between β −Ga nucleation and α −Ga nucleation from the liquid phase is marked by the green star symbols, which could be modeled by the following equation,

$$T^*_{anneal} = T_0[1 - (\sigma_0/\sigma)^\delta], \quad (1)$$

© 2023 Wiley-VCH GmbH

16136829, 0, Downloaded from https://onlinelibrary.wiley.com/doi/10.1002/smll.202305798 by Jie Shang - Ningbo Institute Of Materials , Wiley Online Library on [24/10/2023]. See the Terms and Conditions (https://onlinelibrary.wiley.com/terms-and-conditions) on Wiley Online Library for rules of use; OA articles are governed by the applicable Creative Commons License

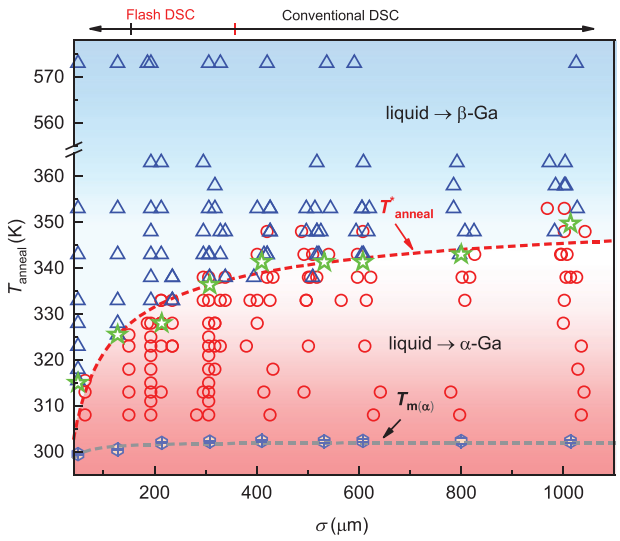

Figure 4. 2D summary plot of polymorph selection on the sample size σ and the annealing temperature T_{anneal}. The margin that differentiates liquid → β (triangles) and liquid → α (circles) is fitted to Equation (1) (see the red dash line). The size dependence of the melting point of the α −Ga is also included at the bottom with a fit to Equation (1).

where T_0, σ_0, and δ are fitting parameters. This equation has been widely used to capture the size dependence of the glass transition temperature for polymeric glasses[51] and metallic glasses.[52] In our case, we identify that $T_0 \approx 357.4$ K, $\sigma_0 \approx 0.81$ μm, and $\delta \approx 0.47$. In theory, T_0 is the upper limit or the saturation temperature ($\sigma \to +\infty$) of the phase transition margin. σ_0 is the lower limit of the sample size to have a vanishing T^*_{anneal}. That means the vanishing of the survival region of α −Ga. Interestingly, a previous study by He et al. revealed that the α −Ga formation is forbidden when the average particle size is 0.8 − 0.6 μm while β −Ga is mainly formed.[23] In other words, with further reducing sample size, the denser packed crystalline phases are favored. This indicates the disfavor of the covalent bonds at a smaller sample size, that is larger surface-to-volume ratio. This is understandable from Figure 1a since the main role of the covalent bonds is as the bridge between the layered densely packed local structures. We also include the melting curve of α −Ga at various sample sizes for comparison. This result is consistent with the previous study by Kumar et al.[43] As shown in Figure 4, it can also be very well described by Equation (1), which shows its generality in describing the sample size dependence of the thermodynamic properties.

As a single-component system, the crystallization of Ga is by no means easy to understand. As we found above, there could be two different crystallization pathways. The liquid phase can crystallize into either α −Ga or β −Ga depending on the annealing temperature T_{anneal}, with α −Ga favored at lower T_{anneal}. This polymorph selection mechanism makes Ga unique among other elements in the periodic table. Whether such kind of polymorph selection mechanism exists or not in other elements, such as Au, Cu, or Hg, is an interesting question to ask. It may depend on the bonding nature in these materials. We are following similar experimental protocol to investigate these additional elements. From the careful crystal structure analysis (see Figure 1 and Table 1), we believe that the covalent bonds play a key role in the crystallization process, that is polymorph selection. The introduction of the covalent bonds in α −Ga gives its distinct structure from the featureless densely packed β −Ga. This in turn gives rise to their different physical properties. We will discuss our findings from the perspective of this bonding nature.

Now we get to know the important role of T_{anneal} in determining the crystallization pathways of liquid Ga. The identification of the critical T_{anneal} is one of our key findings. The phase transition behavior could be linked to the transient evolution of local structural orderings related to covalent bonding, which could survive even in the liquid state. In principal, the covalent bonds should be more energetically favored at lower temperatures. In the current study, it can be roughly characterized by T^*_{anneal}. Since the main difference between α −Ga and β −Ga is the existence or absence of covalent bonds, the covalent bonds must form in the crystallization process to α −Ga. There should be some sort of "driving force" for the formation of the covalent bonds, which shall source from the interatomic interactions. As β −Ga will form at higher temperatures, the formation of covalent bonds is less favored energetically so the driving force will decrease remarkably. Therefore, the driving force we mentioned here actually refers to the energetically favorable degree for the covalent bond formation from the atomic interactions. However, this quantity is very difficult to quantitatively calculate in experiments, which calls for careful calculations from density functional theory in the future.

First of all, when T_{anneal} is much higher than T^*_{anneal}, there is no driving force to form the covalent bonds and the liquid can be treated as a normal simple liquid. The crystallization process is more like an ordinary densification process with β −Ga with full metallic bonds formed, driven by density fluctuations. Density may be the dominant order parameter, even though the pre-ordering effect is also interesting for future study.[53,54] The liquid properties do not rely on T_{anneal}. This explains why T_{xtal} (liquid → β) is invariant to T_{anneal}, the sample size, and the cooling rates (see Figure 2d). Our case is very different from the supercooling phenomenon in water, in which the hydrogen bonds and the resultant local tetrahedral orderings always depend on the temperature and the cooling rate.

On the contrary, at low T_{anneal}, covalent bonds are considerably favored energetically so they can form easily, which facilitates the nucleation and growth of α −Ga. This is why there is only liquid → α −Ga when $T_{anneal} < T^*_{anneal}$. With slightly increasing T_{anneal}, the driving force for the covalent bond formation will decrease remarkably. This causes the plummet of T_{xtal}(liquid → α) since larger undercooling is required to nucleate α −Ga. If the T_{anneal} further increase to slightly higher than T^*_{anneal}, the transition enters the stage where β −Ga is the primary crystalline product from the liquid phase. Nevertheless, some fragmented local structures with covalent bonds can be inherited from the liquid phase in β −Ga. This preordering effect will promote α −Ga nucleation,[53,54] which explains the continuous drop of T_{xtal}($\beta \to \alpha$) close to T^*_{anneal}. Above a certain high temperature where the covalent bond is completely disfavored in the liquid phase, T_{xtal}(liquid → β) becomes invariant to T^*_{anneal} as discussed above.

To further corroborate our ideas, we analyzed the solid–solid phase transformation behavior. **Figure 5** shows the size dependence of T_{xtal}(liquid → β), T_{xtal}($\beta \to \alpha$), and more importantly

© 2023 Wiley-VCH GmbH

16136829, 0, Downloaded from https://onlinelibrary.wiley.com/doi/10.1002/smll.202305798 by Jie Shang - Ningbo Institute Of Materials , Wiley Online Library on [24/10/2023]. See the Terms and Conditions (https://onlinelibrary.wiley.com/terms-and-conditions) on Wiley Online Library for rules of use; OA articles are governed by the applicable Creative Commons License

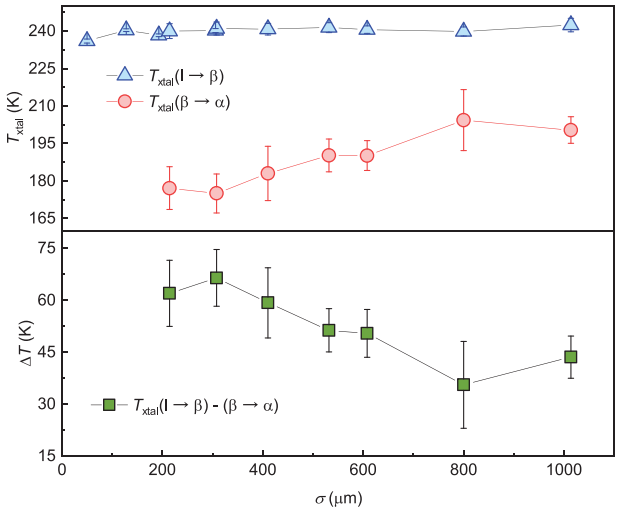

Figure 5. Size-dependent phase transformation temperatures. It is easily observed that the liquid–solid phase transformation temperature T(liquid → β) does not depend on size σ, while the solid–solid phase transformation temperature $T(\beta \rightarrow \alpha)$ increases with increasing size σ. As a consequence, the "undercooling degree" of $\beta \rightarrow \alpha$ phase transition ΔT will decrease with increasing size σ.

their difference $\Delta T(\beta \rightarrow \alpha) = T_{xtal}(\text{liquid} \rightarrow \beta) - T_{xtal}(\beta \rightarrow \alpha)$. As we found above, α −Ga is more stabilized at larger droplet size that benefits from the easier formation of the covalent bonds. This is quite consistent with the tendency of $\Delta T(\beta \rightarrow \alpha)$. From the classical nucleation theory, we note that a reduction in $\Delta T(\beta \rightarrow \alpha)$ indicates the decrease of the thermodynamic driving force of crystallization. This in turn indicates the reduction of the interfacial energy to drive the formation of a critical nucleus, because the less undercooling degree is required for new-phase nucleation if some local structures with a consistent feature as the crystalline product are able to form. In other words, the easier formation of covalent bonds will effectively reduce the liquid-crystal interfacial energy or even the crystallization barrier to facilitate crystallization.

3. Conclusion

In summary, we performed extensive calorimetry experiments for Ga of various sizes at the micron scale. It is interesting to observe two different crystalline phases from the liquid phase. The two domains are separated effectively by the annealing temperature. These results are reasonably understood from the bonding nature that differentiates the two crystalline phases. That is, the formation of covalent bonds will determine the polymorph selection during the crystallization. In addition, the covalent bonds should be of great importance in the nucleation of α −Ga from β −Ga. These results highlight the importance of the covalent bonds in understanding the physical properties of Ga and provide further guidance on the design of new applications. Interestingly, it was recently reported that the passive oxide surface layer will help increase the supercooling capability of Ga particles.[47] It would be interesting in the future study to unveil how the oxide layer would affect the polymorph selection mechanism of liquid Ga at small length scales.

Our findings indicate that there may exist two different phases in the liquid state,[55] depending on the absence/appearance of the covalent bonds. This hints the existence of a possible liquid–liquid phase transition in a certain temperature range. However, because of the low fraction of covalent bonds in the unit cell of α −Ga, the signal can be rather subtle, which brings the main experimental difficulty. Some trial experiments are on the way and the results will be reported somewhere else. Such kind of explorations may bring some new horizons to understanding the liquid–liquid phase transition in matters. With a well-designed sample size based on the current findings, Ga might be a reasonably good prototypical material to unravel the mystery of liquid–liquid phase transition. This calls for careful future computational study and experimental characterization.

4. Experimental Section

Materials: High-purity Ga (Ga pellets, 6 mm diameter, 99.99999%, Alfa Assar) initially in the solid phase at the room temperature was used in the experiments. The oxide film on the surface was carefully removed before sample preparation. Specifically, a surgical knife was used to cut off the surface layer of gallium to remove the thin oxide layer on the surface. This study notes that the nanometer-scale native oxide layer cannot be avoided completely. It actually encapsulated the pure substance to prevent it from heterogeneous nucleation,[47] which enabled to study the phase transformation behaviors of pure gallium. Sitting on the external surface, liquid gallium without any oxide layer will always easily crystallize to α −Ga, assisted by heterogeneous nucleation. The initial phase α −Ga of solid was identified by FEI QUANTA FEG 250 integrated with an Oxford Electron Backscattering Diffraction (EBSD) system operated at 20 kV and controlled by Aztec Oxford data collection software . Figure S6a (Supporting Information) shows the typical EBSD pattern well indexed with α −Ga orthorhombic lattice direction.

Preparation of thermal analysis samples: For DSC measurements, the Ga ball was divided into small particles with different quality. Once the particles were heated above the melting point, due to the large surface tension of Ga, liquid particles tend to agglomerate into spheres. The optical microscope images of Ga sample before and after annealed respectively are shown in Figure S6b,c (Supporting Information). For the convenience of calculation, the particles were approximated to be spherical. The droplet diameter was measured to characterize the droplet size according to the mass and density of liquid Ga. For Flash DSC measurements, Ga was first cut into particles of approximate target size under a microscope, and then calculated the exact mass of the test sample based on the actual heat value absorbed during the melting process and the unit mass melting enthalpy of α −Ga, then using the same method as in DSC to obtain the actual size.

Thermal analyses measurements: Thermal analyses were done on a differential scanning calorimetry instrument (DSC, DSC214, Netzsch for $\sigma \approx$ 214, 308, 410, 532, 608, 1014 μm and Flash DSC1+, Mettler Toledo for $\sigma \approx$ 50, 128, 193, 306 μm). According to the melting point (T_m) and the latent heat of phase change (ΔH_f) during the test process, the liquid–solid/solid–solid transition behavior could be judged in the previous cooling segment. The low-temperature limits of NETZSCH instrument differential scanning calorimetry (DSC) 214 calorimeter was 123 K under liquid nitrogen refrigeration mode. The Al_2O_3 pan was used and the experiments was carried out at $\phi_h = \phi_c = 0.083$ K s^{-1} DSC 214 in a nitrogen protected ambient. Flash differential scanning calorimetry (Flash DSC) experiments were performed by using a Mettler–Toledo Flash DSC1+ equipped with the UFH sensor, the lower-temperature limit was 183 K. The sample was loaded on the chip sensor (USF-1) and measured at ϕ_h = 0.083 K s^{-1}, ϕ_c = 0.083, 0.83, 8.3 K s^{-1} under argon gas flowed with a constant rate of 80 mL min^{-1}.

© 2023 Wiley-VCH GmbH

16136829, 0, Downloaded from https://onlinelibrary.wiley.com/doi/10.1002/smll.202305798 by Jie Shang - Ningbo Institute Of Materials , Wiley Online Library on [24/10/2023]. See the Terms and Conditions (https://onlinelibrary.wiley.com/terms-and-conditions) on Wiley Online Library for rules of use; OA articles are governed by the applicable Creative Commons License

Supporting Information

Supporting Information is available from the Wiley Online Library or from the author.

Acknowledgements

The authors thank Prof. Haibin Yu and Prof. Haiyang Niu for assistance in the experiment and valuable discussions, and Dr. Shaozhu Xiao and Dr. Ri He for help in software learning. This work was partially supported by the National Natural Science Foundation of China (U22A20248, U1909215, 52127803, U20A6001, 51931011, 51971233, 62174165, M-0152, U22A2075, 52105286, 52201236, 62204246, 92064011, and 62174164), the External Cooperation Program of Chinese Academy of Sciences (174433KYSB20190038 and 174433KYSB20200013), the Instrument Developing Project of the Chinese Academy of Sciences (YJKYYQ20200030), K.C. Wong Education Foundation (GJTD-2020-11), the Chinese Academy of Sciences Youth Innovation Promotion Association (2018334), the "Pioneer" and "Leading Goose" R&D Program of Zhejiang (2022C01032), Zhejiang Provincial Key R&D Program (2021C01183), the Key Research and Development Project of Zhejiang Province (2021C01039), the Natural Science Foundation of Zhejiang Province (LD22E010002), "High-level talent special support plan" technology innovation leading talent project of Zhejiang Province (2022R52004), the Ningbo Scientific and Technological Innovation 2025 Major Project (2020Z022) and the Ningbo Natural Science Foundations (20221JCGY010312).

Conflict of Interest

The authors declare no conflict of interest.

Data Availability Statement

The data that support the findings of this study are available from the corresponding author upon reasonable request.

Keywords

crystallization, phase transformation, size effect, supercooled liquid, thermal treatment

Received: July 10, 2023
Revised: October 8, 2023
Published online:

[1] T. Daeneke, K. Khoshmanesh, N. Mahmood, I. A. De Castro, D. Esrafilzadeh, S. Barrow, M. Dickey, K. Kalantar-Zadeh, *Chem. Soc. Rev.* **2018**, *47*, 4073.
[2] D. Pierre, *Ind. Eng. Chem.* **1964**, *56*, 54.
[3] C. Wang, C. Wang, Z. Huang, S. Xu, *Adv. Mater.* **2018**, *30*, 1801368.
[4] J. Yan, Y. Lu, G. Chen, M. Yang, Z. Gu, *Chem. Soc. Rev.* **2018**, *47*, 2518.
[5] Y. Lin, J. Genzer, M. D. Dickey, *Adv. Sci.* **2020**, *7*, 2000192.
[6] H. Song, T. Kim, S. Kang, H. Jin, K. Lee, H. J. Yoon, *Small* **2020**, *16*, 1903391.
[7] S.-Y. Tang, C. Tabor, K. Kalantar-Zadeh, M. D. Dickey, *Annu. Rev. Mater. Res.* **2021**, *51*, 381.
[8] E. Shchukina, M. Graham, Z. Zheng, D. Shchukin, *Chem. Soc. Rev.* **2018**, *47*, 4156.
[9] S.-H. Byun, J. Y. Sim, Z. Zhou, J. Lee, R. Qazi, M. C. Walicki, K. E. Parker, M. P. Haney, S. H. Choi, A. Shon, G. B. Gereau, J. Bilbily, S. Li, Y. Liu, W. H. Yeo, J. G. McCall, J. Xiao, J. W. Jeong, *Sci. Adv.* **2019**, *5*, eaay0418.
[10] H. Wang, S. Chen, X. Zhu, B. Yuan, X. Sun, J. Zhang, X. Yang, Y. Wei, J. Liu, *Matter* **2022**, *5*, 2054.
[11] X. Wang, X. Li, M. Duan, S. Shan, X. Zhu, Y. Chai, H. Wang, X. Sun, L. Sheng, G. Qing, W. Rao, L. Hu, J. Chen, J. Liu, *Matter* **2022**, *5*, 219.
[12] Z. Yu, J. Shang, X. Niu, Y. Liu, G. Liu, P. Dhanapal, Y. Zheng, H. Yang, Y. Wu, Y. Zhou, Y. Wang, D. Tang, R.-W. Li, *Adv. Electron. Mater.* **2018**, *4*, 1800137.
[13] M. H. Malakooti, N. Kazem, J. Yan, C. Pan, E. J. Markvicka, K. Matyjaszewski, C. Majidi, *Adv. Funct. Mater.* **2019**, *29*, 1906098.
[14] B. Wang, J. Maslik, O. Hellman, A. Gumiero, K. Hjort, *Adv. Funct. Mater.* **2023**, 2300036.
[15] X. G. Gong, G. L. Chiarotti, M. Parrinello, E. Tosatti, *Phys. Rev. B* **1991**, *43*, 14277.
[16] M. Bernasconi, G. L. Chiarotti, E. Tosatti, *Phys. Rev. B* **1995**, *52*, 9988.
[17] L. Bosio, A. Defrain, H. Curien, A. Rimsky, *Acta Crystallogr., Sect. B: Struct. Crystallogr. Cryst. Chem.* **1969**, *25*, 995.
[18] L. Bosio, H. Curien, M. Dupont, A. Rimsky, *Acta Crystallogr., Sect. B: Struct. Crystallogr. Cryst. Chem.* **1972**, *28*, 1974.
[19] L. Bosio, H. Curien, M. Dupont, A. Rimsky, *Acta Crystallogr., Sect. B: Struct. Crystallogr. Cryst. Chem.* **1973**, *29*, 367.
[20] L. Bosio, *J. Chem. Phys.* **1978**, *68*, 1221.
[21] O. Züger, U. Dürig, *Phys. Rev. B* **1992**, *46*, 7319.
[22] D. A. Walko, I. K. Robinson, C. Grütter, J. H. Bilgram, *Phys. Rev. Lett.* **1998**, *81*, 626.
[23] H. He, G. T. Fei, P. Cui, K. Zheng, L. M. Liang, Y. Li, L. De Zhang, *Phys. Rev. B* **2005**, *72*, 073310.
[24] X. F. Li, G. T. Fei, X. M. Chen, Y. Zhang, K. Zheng, X. L. Liu, L. D. Zhang, *Europhys. Lett.* **2011**, *94*, 16001.
[25] Z. Liu, Y. Bando, M. Mitome, J. Zhan, *Phys. Rev. Lett.* **2004**, *93*, 095504.
[26] M. Losurdo, A. Suvorova, S. Rubanov, K. Hingerl, A. S. Brown, *Nat. Mater.* **2016**, *15*, 995.
[27] L. Bosio, C. G. Windsor, *Phys. Rev. Lett.* **1975**, *35*, 1652.
[28] A. Di Cicco, *Phys. Rev. Lett.* **1998**, *81*, 2942.
[29] J. Wolny, S. Nizioł, W. Łużny, L. Pytlik, J. Sołtys, R. Kokoszka, *Solid State Commun.* **1986**, *58*, 573.
[30] D. Campanini, Z. Diao, A. Rydh, *Phys. Rev. B* **2018**, *97*, 184517.
[31] X. Gong, G. Chiarotti, M. Parrinello, E. Tosatti, *Europhys. Lett.* **1993**, *21*, 469.
[32] K.-H. Tsai, T.-M. Wu, S.-F. Tsay, *J. Chem. Phys.* **2010**, *132*, 034502.
[33] L. H. Xiong, X. D. Wang, Q. Yu, H. Zhang, F. Zhang, Y. Sun, Q. P. Cao, H. L. Xie, T. Q. Xiao, D. X. Zhang, C. Z. Wang, K. M. Ho, Y. Ren, J. Z. Jiang, *Acta Mater.* **2017**, *128*, 304.
[34] L. Peng, E. Chen, S. Liu, X. Liu, Y. Yu, *Phys. Rev. B* **2019**, *100*, 104113.
[35] P. H. Poole, F. Sciortino, U. Essmann, H. E. Stanley, *Nature* **1992**, *360*, 324.
[36] S. Sastry, C. Austen Angell, *Nat. Mater.* **2003**, *2*, 739.
[37] Y. Katayama, T. Mizutani, W. Utsumi, O. Shimomura, M. Yamakata, K.-i. Funakoshi, *Nature* **2000**, *403*, 170.
[38] C. Tien, E. V. Charnaya, W. Wang, Y. A. Kumzerov, D. Michel, *Phys. Rev. B* **2006**, *74*, 024116.
[39] D. A. Carvajal Jara, M. Fontana Michelon, A. Antonelli, M. de Koning, *J. Chem. Phys.* **2009**, *130*, 221101.
[40] R. Li, L. Li, T. Yu, L. Wang, J. Chen, Y. Wang, Z. Cai, J. Chen, M. L. Rivers, H. Liu, *Appl. Phys. Lett.* **2014**, *105*, 041906.
[41] R. Li, G. Sun, L. Xu, *J. Chem. Phys.* **2016**, *145*, 054506.
[42] W. Luzny, S. Niziol, J. Mayer, I. Natkaniec, *Phys. Status Solidi A* **1989**, *116*, 1 K25.
[43] V. B. Kumar, Z. Porat, A. Gedanken, *J. Therm. Anal. Calorim.* **2015**, *119*, 1587.

© 2023 Wiley-VCH GmbH

16136829, 0, Downloaded from https://onlinelibrary.wiley.com/doi/10.1002/smll.202305798 by Jie Shang - Ningbo Institute Of Materials , Wiley Online Library on [24/10/2023]. See the Terms and Conditions (https://onlinelibrary.wiley.com/terms-and-conditions) on Wiley Online Library for rules of use; OA articles are governed by the applicable Creative Commons License

[44] S.-Y. Tang, D. R. G. Mitchell, Q. Zhao, D. Yuan, G. Yun, Y. Zhang, R. Qiao, Y. Lin, M. D. Dickey, W. Li, *Matter* **2019**, *1*, 192.
[45] C. Zhang, L. Li, X. Yang, J. Shi, L. Gui, J. Liu, *Int. J. Heat Mass Transf.* **2020**, *148*, 119055.
[46] M. Yunusa, A. Adaka, A. Aghakhani, H. Shahsavan, Y. Guo, Y. Alapan, A. Jákli, M. Sitti, *Adv. Mater.* **2021**, *33*, 2104807.
[47] I. D. Joshipura, C. K. Nguyen, C. Quinn, J. Yang, D. H. Morales, E. Santiso, T. Daeneke, V. K. Truong, M. D. Dickey, *iScience* **2023**, *26*, 106493.
[48] V. Heine, *J. Phys. C: Solid State Phys.* **1968**, *1*, 222.
[49] M. Chase, C. Davies, J. Downey, *J. Phys. Chem. Ref. Data, Monograph* **1998**, 1952.
[50] T. S. Ingebrigtsen, T. B. Schrøder, J. C. Dyre, *Phys. Rev. X* **2012**, *2*, 011011.
[51] J. A. Forrest, K. Dalnoki-Veress, J. R. Stevens, J. R. Dutcher, *Phys. Rev. Lett.* **1996**, *77*, 2002.
[52] Y. Z. Li, Y. T. Sun, Z. Lu, M. Z. Li, H. Y. Bai, W. H. Wang, *J. Chem. Phys.* **2017**, *146*, 224502.
[53] Y.-C. Hu, H. Tanaka, *Sci. Adv.* **2020**, *6*, eabd2928.
[54] Y.-C. Hu, H. Tanaka, *Nat. Commun.* **2022**, *13*, 4519.
[55] H. Tanaka, *J. Chem. Phys.* **2020**, *153*, 130901.

© 2023 Wiley-VCH GmbH

16136829, 0, Downloaded from https://onlinelibrary.wiley.com/doi/10.1002/smll.202305798 by Jie Shang - Ningbo Institute Of Materials , Wiley Online Library on [24/10/2023]. See the Terms and Conditions (https://onlinelibrary.wiley.com/terms-and-conditions) on Wiley Online Library for rules of use; OA articles are governed by the applicable Creative Commons License